IEEE Access
Multidisciplinary : Rapid Review : Open Access Journal

Received October 3, 2019, accepted October 20, 2019, date of publication October 30, 2019, date of current version November 12, 2019.

Digital Object Identifier 10.1109/ACCESS.2019.2950429

Machine Current Sensor FDI Strategy in PMSMs

HAIBO LI, (Student Member, IEEE), YI QIAN, (Fellow, IEEE), SOHRAB ASGARPOOR, (Senior Member, IEEE), AND HAMID SHARIF, (Fellow, IEEE)

Electrical and Computer Engineering Department, University of Nebraska–Lincoln, Lincoln, NE 68588-0511, USA

Corresponding author: Haibo Li (harbor.lee@huskers.unl.edu)

ABSTRACT This work proposes a machine current sensor fault detection and isolation (FDI) strategy in permanent magnet synchronous machines (PMSMs) resilient to multiple faults. The fault detection is performed by comparing the measured and estimated DC link currents. The fault isolation is achieved according to machine phase signal estimation and the corresponding residual examination. Single sensor fault, multiple sensor faults and non-sensor fault are covered by the proposed FDI method. The proposed sensor FDI method is not influenced by machine imbalance, feasible for FDI of both single and multiple machine current sensor faults, and capable of distinguishing between machine current sensor fault and non-sensor fault. The proposed method is validated with simulation studies in MATLAB, and the studies demonstrate that the proposed machine current sensor FDI method, different from existing methods, has a unique feature of being able to handle multiple sensor faults with the consideration of non-sensor fault disturbance.

INDEX TERMS Current sensor, fault detection and isolation (FDI), multiple faults, non-sensor fault, PMSM.

I. INTRODUCTION

A variety of power equipment influences the performance of electric power grid including electric machines, transmission lines, transformers, etc. [1]–[3], of which the electric machines have an critical role in the electric power quality and power system reliability. However, different faults, including winding fault, inverter fault and sensor fault, deteriorate the electric machine control, which could influence the electric grid. The sensor fault in particular is a common fault scenario. According to a survey for electric machine system failures in Swedish wind application, system failures caused by sensor faults count 14.1% out of the total failures, meaning that these sensors in the system are very vulnerable devices [4]. Therefore, it is of great importance to identify a sensor fault which helps to avoid the machine system failure under sensor fault occurrence.

Among different sensor faults, the machine current sensor fault is important as the sensor measurement is fed into control system directly and a faulty signal could cause significant error in the control command. To mitigate the impact of this type of fault, a machine current sensor fault detection and isolation (FDI) strategy is highly desirable. An easy and straightforward way is to add more sensors and perform FDI with sensor redundancy. However, this redundancy brings more cost, weight, as well as hardware complexity. To get rid of these disadvantages, much effort has been put to develop sensor FDI methods with analytical sensor redundancies. In [5], a Luenberger state observer-based method is proposed which is developed from machine model. A residual between the estimated and measured information is used for sensor FDI. However, the Luenberger state observer is sensitive to system parameter variations which happens under changing environment temperature and machine system aging. The authors in [6] propose a fuzzy logic method. This sensor FDI method however needs the Takagi-Sugeno fuzzy state observers which are hard to design. The authors in [7] propose a method with model-based neural network (NN) observers to estimate current or voltage, which is later compared to sensor signals for the FDI in a permanent magnet synchronous machine (PMSM)-based wind energy system. A backpropagation algorithm is used here for training the NN. However, this algorithm training is time-consuming and it is challenging to obtain accurate estimation data from NN observers under a fast-changing machine operating condition. The authors in [8]–[11] propose machine current sensor FDI methods with sliding-mode control, higher order sliding mode (HOSM) observer, extended Kalman filter, etc. The machine systems with sensor FDI methods developed in these works are capable of adaptively

The associate editor coordinating the review of this manuscript and approving it for publication was Dwarkadas Pralhaddas Kothari.

reorganizing themselves in the occurrence of current sensor fault, such as achieving seamless transition from vector control to fuzzy-logic-based intelligent control. However, it is hard for the proposed methods to handle multiple sensor faults, because the underlying assumption of these FDI methods is that there is only one sensor fault, and the machine has to operate under open-loop Volts/Hertz control when multiple faults occur which results in a significant performance degradation.

Additionally, for most existing methods in literature, the machine current is estimated by model-based observers for comparison with the sensor-measured signal to perform the current sensor FDI. It is assumed in these works that the residual increase, if occurred, is caused by sensor measurement fault while the estimated signal is correct, which however is not always true in practice. If the estimation fault is considered, an additional layer of redundancy must be incorporated into the FDI method. Compared to the methods presented in [5]–[11], a method based on three-phase balance is proposed in [12], [13] for machine current sensor FDI, which is very easy to implement. However, this approach is only valid for a balanced three-phase system and the FDI method will fail if an imbalance exists [14], which can be caused by faults in various machine system components, such as bearing, shaft, etc. The work in [15] proposes an offline test-based method to detect and isolate machine current sensor offset or gain drift fault. A system shutdown is required in this method to perform the sensor FDI, which obviously is not always practical in reality considering that a fault could happen anytime when the machine system is running. The authors in [16] propose an FDI scheme feasible for multiple sensor failures in a motor system by adding an additional dc link current sensor. The presented work can be very helpful to handle the current sensor and position sensor faults at the same time without disturbing the continuous machine operation. However, the two machine current sensor faults and non-sensor fault(s) scenarios are not considered. False detection could happen when these fault scenarios exist. Similar disadvantage of either multiple machine current sensor faults or non-sensor fault(s) disturbance exists for the sensor FDI methods presented in [17]–[21]. The authors in [22] and [23] propose a FDI method based on the source current residual, which could potentially be used for various machine current sensor fault scenarios considering the disturbance of a non-sensor imbalance in PMSMs. However, the multiple machine current sensor faults are not well covered. False isolation would occur if these multiple current sensor faults are not well addressed.

FDI of multiple machine current sensor faults under the disturbance of various non-sensor faults, such as machine imbalance, has been a challenging issue in electric machines which is not addressed in literature. This work proposes a sensor FDI method which addresses the shortcomings or limitations of the methods reviewed earlier. The proposed method requires at most one additional current sensor in the DC link if the PMSM system is powered by a separate DC source, or requires no additional sensor if the system is grid-tied. The proposed method does not require complicated modeling, is not influenced by machine three-phase imbalance, is resilient to multiple machine current sensor faults, and is capable of distinguishing between machine current sensor and non-sensor faults.

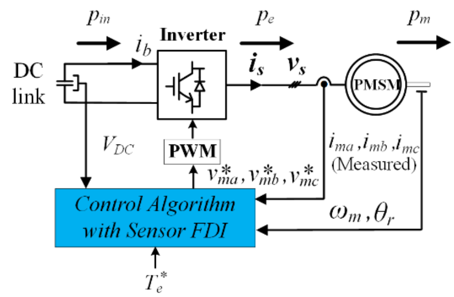

FIGURE 1. Overview of a PMSM system with sensor FDI.

TABLE 1. Machine current sensor and non-sensor faults summary.

Fault type	Fault scenario		
Machine current sensor fault(s)	Single sensor fault		Phase A fault
			Phase B fault
			Phase C fault
	Multiple sensor faults	Two phase faults	Phase A and B faults
			Phase B and C faults
			Phase A and C faults
		Three phase faults	Phase A, B and C faults
Non-sensor fault(s)	Three-phase imbalance		
	Inverter fault		
	Other non-sensor faults		

II. PROPOSE PMSM CURRENT SENSOR FDI METHOD

An overview of a PMSM system with sensor FDI is shown in Fig. 1. Control commands are calculated under specific torque T_e^*, DC link battery voltage V_{DC} and machine mechanical speed ω_{m}. It is clear in Fig. 1 that the sensor measurements of three phase machine current are fed into the control system which are used directly for control command calculation. The fault in current sensor measurements will cause incorrect command generation which challenges the PMSM system performance. To mitigate the influence of machine current sensor fault(s), it is highly desirable to develop and integrate a sensor FDI method into the machine control algorithm. The summary of single/multiple machine current sensor faults and single non-sensor fault scenarios are presented in Table 1. A current sensor fault could happen in each of the three phases. Also, different phases could present sensor faults at the same time. Non-sensor faults, such as three-phase imbalance, power inverter fault, etc., sometimes also exist in a machine system. Different features could be observed under these faults which will be further explained below.

A. SENSOR FAULT DETECTION

Different power components showing the PMSM system power flow are marked in Fig. 1, where p_{in}, p_e and p_m are the DC link power, PMSM input electrical power, and output mechanical power, respectively. According to the power balance principle,

$$p_{in} = p_e + p_{inv,loss} \tag{1}$$

where $p_{inv,loss}$ is the inverter power loss. The DC link is assumed to be a storage battery in this study with current i_b going through it, and therefore p_{in} can be derived as

$$p_{in} = V_{DC} i_b \tag{2}$$

where V_{DC} is the measured battery voltage at the DC link. The PMSM input electrical power p_e can be calculated as

$$p_e = \frac{3}{2}(v_d i_d + v_q i_q) \tag{3}$$

where v_d and v_q are the voltages, and i_d and i_q are the currents in $d-$ and q–axis respectively in dq-axis synchronously rotating reference frame. The inverter loss can be estimated based on the semiconductor device parameters in datasheet with linear interpolation considering the influences of temperature. The power loss in (1) is mostly due to the semiconductor losses that can be derived as

$$p_{inv,loss} = \sum_{n=1}^{N} (p_{con} + p_{sw}) \tag{4}$$

where N is the total number of the semiconductor devices in the inverter; p_{con} and p_{sw} are the conduction and switching losses of one semiconductor device, respectively. According to (1)-(4), the DC link battery current is given by

$$\widehat{i_b} = \frac{p_{in}}{V_{DC}} = \frac{p_e + p_{inv,loss}}{V_{DC}} = \frac{p_e + \sum_{n=1}^{N} (p_{con} + p_{sw})}{V_{DC}} \tag{5}$$

where $\hat{i_b}$ is the estimated DC link battery current. For each device, the power loss is calculated as

$$p_{con} = \frac{1}{T_s} \int [V_T + R_{on} i_D] i_D dt \tag{6}$$

$$p_{sw} = \frac{(E_{on} + E_{off})}{T_s} \times \frac{i_D}{I_N} \times \frac{V_{DC}}{V_N} \tag{7}$$

where V_T, R_{on}, i_D, E_{on}, E_{off}, T_s, I_N and V_N are the device threshold voltage, on-state resistance, device current , the switching loss under the rated current and voltage condition in one turn-on process, the switching loss under the rated current and voltage condition in one turn-off process, switching period, device rated current, and device rated voltage, respectively [24]. Based on the previous analysis, the DC link battery current can be estimated. A DC link current residual thereby is calculated as

$$r_{ib} = \left| i_b - \widehat{i_b} \right| \tag{8}$$

This residual is an indicator in the proposed method to tell if a fault exists. Fig. 2 shows the proposed PMSM current sensor fault detection method. If no fault exists, the DC link battery currents by measurement and estimation should be equal, i.e., $r_{ib} \approx 0$. If a machine current sensor fault exists, the estimated $\widehat{i_b}$ based on the incorrect sensor signal would deviate from the measured value. This results in an inequality between the DC link battery current measurement and estimation, which leads to a significant increase in r_{ib}. Consequently, a threshold value δ_{ib} could be defined to compare with DC link current residual r_{ib} for the fault detection. If this pre-defined δ_{ib} is exceeded by r_{ib}, there is a fault in the machine system. Otherwise, no sensor fault is reported.

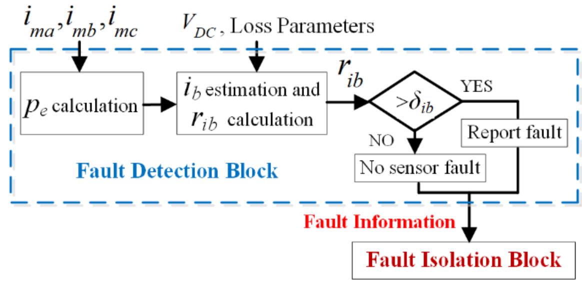

FIGURE 2. Proposed fault detection method.

It is inevitable to have some loss estimation errors due to the system parameter errors and the influence of ambient environment such as temperature. This error issue however could be handled by selecting a proper fault detection threshold, which is related to the method sensitivity to faults. When a high threshold value is selected, the proposed fault detection method will present high tolerance to system parameter errors as well as environmental influence, which is helpful to reduce the false detection rate during the FDI implementation. On the other hand, a high threshold selection will result in a compromised detection sensitivity in terms of some early-stage faults which usually are not severe.

B. SENSOR FAULT ISOLATION

The fault detection tells if there is a sensor fault, however this process could not identify which location presents the fault. To isolate the specific sensor fault location, a fault isolation method based on phase signal estimation and residual examination is proposed, which is given in Fig. 3. The PMSM phase currents can be written as

$$\begin{aligned} i_{ma}(t) &= i_m \cos(\omega_e t + \varphi) \\ i_{mb}(t) &= i_m \cos(\omega_e t + \varphi - \frac{2\pi}{3}) \\ i_{mc}(t) &= i_m \cos(\omega_e t + \varphi + \frac{2\pi}{3}) \end{aligned} \tag{9}$$

The quantity of one phase can be used to estimate the current in other phases. For example, phase B and C currents i_{mb} and i_{mc} can be estimated from measured phase A current i_{ma} as

$$\widehat{i}_{mb,a}(t) = i_{ma}(t - \frac{2\pi}{3\omega_e}) \tag{10}$$

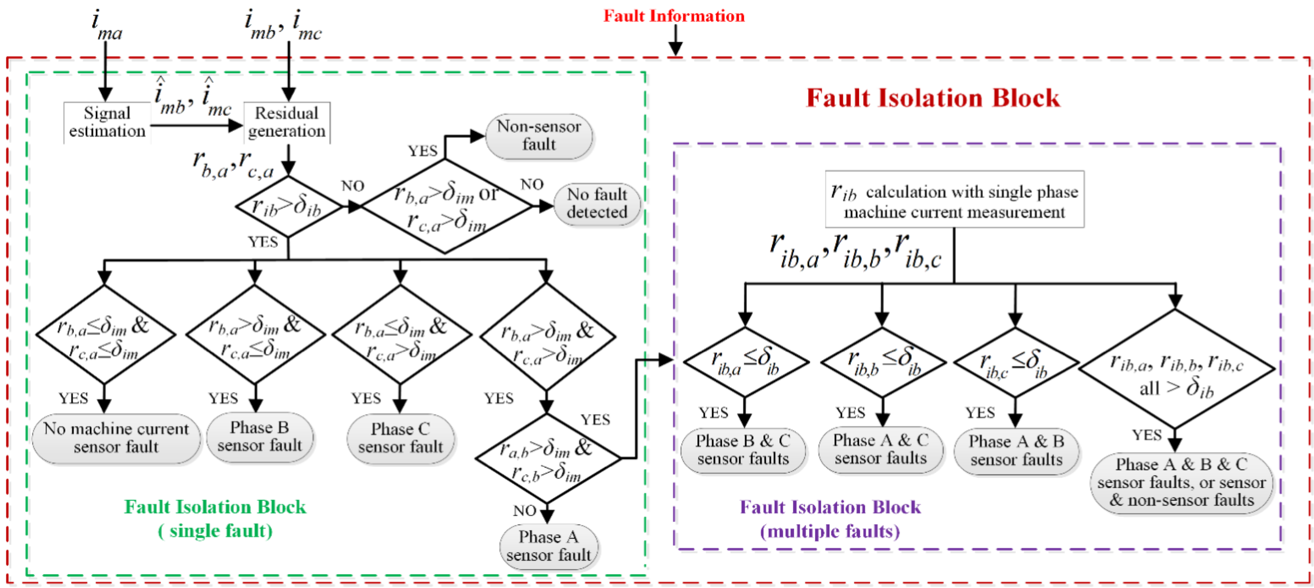

FIGURE 3. Proposed fault isolation method.

$$\hat{i}_{mc,a}(t) = i_{ma}(t - \frac{4\pi}{3\omega_e}) \tag{11}$$

These estimations $\hat{i}_{mb,a}$ and $\hat{i}_{mc,a}$ are used for comparison to sensor measurements i_{mb} and i_{mc} which generate two residuals $r_{b,a}$ and $r_{c,a}$ as

$$r_{b,a} = \left|i_{mb}(t) - \hat{i}_{mb,a}(t)\right| = \left|i_{mb}(t) - i_{ma}(t - \frac{2\pi}{3\omega_e})\right| \tag{12}$$

$$r_{c,a} = \left|i_{mc}(t) - \hat{i}_{mc,a}(t)\right| = \left|i_{mc}(t) - i_{ma}(t - \frac{4\pi}{3\omega_e})\right| \tag{13}$$

The value of measured phase B current i_{mb} can also be used to estimate the values of i_{ma} and i_{mc} so as to obtain the $\hat{i}_{ma,b}$ and $\hat{i}_{mc,b}$, from which another two residuals $r_{a,b}$ and $r_{c,b}$ can thereby be generated as

$$r_{a,b} = \left|i_{ma}(t) - \hat{i}_{ma,b}(t)\right| = \left|i_{ma}(t) - i_{mb}(t - \frac{4\pi}{3\omega_e})\right| \tag{14}$$

$$r_{c,b} = \left|i_{mc}(t) - \hat{i}_{mc,b}(t)\right| = \left|i_{mc}(t) - i_{mb}(t - \frac{2\pi}{3\omega_e})\right| \tag{15}$$

The fault isolation is performed by comparing these different residuals with a tunable threshold δ_{im}, which is summarized in Table 2. Fault isolation of single fault and multiple faults are implemented sequentially in the proposed fault isolation method, as presented in Fig. 3. If the fault detection block returns a residual $r_{ib} > \delta_{ib}$, additional machine current residuals examination is performed as follows.

(a) If $r_{b,a} \le \delta_{im}$ and $r_{c,a} \le \delta_{im}$, there is no machine current sensor fault in phase A, B or C;

(b) If $r_{b,a} > \delta_{im}$ and $r_{c,a} \le \delta_{im}$, the fault is in phase B sensor;

(c) If $r_{b,a} \le \delta_{im}$ and $r_{c,a} > \delta_{im}$, the fault is in phase C sensor;

TABLE 2. Sensor fault isolation rules.

DC link current residual	Machine current residuals				Fault(s) location
r_{ib}	$r_{b,a}$	$r_{c,a}$	$r_{a,b}$	$r_{c,b}$	
$> \delta_{ib}$	$\le \delta_{im}$	$\le \delta_{im}$	–	–	No machine current sensor fault
	$> \delta_{im}$	$\le \delta_{im}$	–	–	Phase B sensor
	$\le \delta_{im}$	$> \delta_{im}$	–	–	Phase C sensor
	$> \delta_{im}$	$> \delta_{im}$	$> \delta_{im}$	$\le \delta_{im}$	Phase A sensor
			$> \delta_{im}$	$> \delta_{im}$	Multiple phases
$\le \delta_{ib}$	$\le \delta_{im}$	$\le \delta_{im}$	–	–	No sensor fault
	$r_{b,a} > \delta_{im}$ or $r_{c,a} > \delta_{im}$				Imbalance fault

(d) If $r_{b,a} > \delta_{im}$ and $r_{c,a} > \delta_{im}$, the fault is in phase A sensor or multiple faults exists in the system.

For case (a), there is a fault other than machine current sensor fault that causes an incorrect calculation of r_{ib}, such as circulating current inside the power inverter [25]. For the case (d), signal estimation from either phase B or phase C sensor measurement and the corresponding residuals will be needed to further isolate the fault(s). For example, residuals $r_{a,b}$ and $r_{c,b}$ can be used. If only $r_{a,b}$ exceeds δ_{im}, the fault is in phase A; otherwise, if both $r_{a,b}$ and $r_{c,b}$ exceed δ_{im}, multiple faults exist. For multiple faults isolation, calculation of DC link battery current residual with single phase machine current sensor measurement is required. Each phase current measurement, together with the corresponding estimated signals of the other two phases, can be used to calculate a DC link current residual. For example, the residual $r_{ib,a}$ can be generated using similar method as calculating r_{ib}, with phase A current sensor signal i_{ma}, and the estimated values $\hat{i}_{mb,a}$

and $\widehat{i}_{mc,a}$. The residual $r_{ib,a}$ could be written as

$$r_{ib,a} = f(i_{ma}(t), \widehat{i}_{mb,a}(t), \widehat{i}_{mc,a}(t)) \tag{16}$$

Similarly, residual $r_{ib,b}$ and $r_{ib,c}$ can be generated with phase B or C current sensor signal, respectively, which could be written as

$$r_{ib,b} = f(\widehat{i}_{ma,b}(t), i_{mb}(t), \widehat{i}_{mc,b}(t)) \tag{17}$$

$$r_{ib,c} = f(\widehat{i}_{ma,c}(t), \widehat{i}_{mb,c}(t), i_{mc}(t)) \tag{18}$$

Double check of $r_{ib,a}$, $r_{ib,b}$ and $r_{ib,c}$ helps isolate the two machine current sensor faults, and also tells if there are three sensor faults or co-existence of sensor and non-sensor faults.

(a) If $r_{ib,a} > \delta_{ib}$, $r_{ib,b} > \delta_{im}$, and $r_{ib,c} \leq \delta_{im}$, the faults are in phase A sensor and phase B sensor;
(b) If $r_{ib,a} > \delta_{ib}$, $r_{ib,b} \leq \delta_{im}$, and $r_{ib,c} > \delta_{im}$, the faults are in phase A sensor and phase C sensor;
(c) If $r_{ib,a} \leq \delta_{ib}$, $r_{ib,b} > \delta_{im}$, and $r_{ib,c} > \delta_{im}$, the faults are in phase B sensor and phase C sensor;
(d) If $r_{ib,a} > \delta_{ib}$, $r_{ib,b} > \delta_{im}$, and $r_{ib,c} > \delta_{im}$, the faults are in all three phase sensors, or there is co-existence of sensor and non-sensor faults.

There are different types of non-sensor faults that could happen in an electric machine system, such as semiconductor device fault, machine imbalance, etc. For the semiconductor device fault, it might lead to a wrong battery current estimation if there is circulating current inside the inverter. This kind of fault will return a $r_{ib} > \delta_{ib}$, but the following isolation process will further check $r_{a,b}$ and $r_{c,b}$ which will return information of no machine current sensor fault based on Table 2. Additional method could be adopted to isolate semiconductor device fault, like thermography [26]. For a non-sensor fault of machine imbalance, the fault detection will return a $r_{ib} < \delta_{ib}$ because the power conservation principle is always valid, but the fault isolation process will return information of $r_{a,b} > \delta_{im}$ or/and $r_{c,b} > \delta_{im}$ if there are waveform distortions in the machine currents.

When there is a co-existence of machine current sensor and non-sensor imbalance faults, additional DC link battery current residuals must be generated with a combination of two phase sensor-measured signals and one phase estimated signal. For example, r_{ib,a,b,c_a} can be generated with phase A and B current sensor-measured i_{ma} and i_{mb}, and phase C current estimated based on phase A as

$$r_{ib,a,b,c\_a} = f(i_{ma}(t), i_{mb}(t), \widehat{i}_{mc,a}(t)) \tag{19}$$

Replacing the estimated phase C current from phase A in above equation with an estimated value from phase B, r_{ib,a,b,c_b} is obtained as

$$r_{ib,a,b,c\_b} = f(i_{ma}(t), i_{mb}(t), \widehat{i}_{mc,b}(t)) \tag{20}$$

Similarly, four more residuals are obtained as

$$r_{ib,a,b\_a,c} = f(i_{ma}(t), \widehat{i}_{mb,a}(t), i_{mc}(t)) \tag{21}$$

$$r_{ib,a,b\_c,c} = f(i_{ma}(t), \widehat{i}_{mb,c}(t), i_{mc}(t)) \tag{22}$$

$$r_{ib,a\_b,b,c} = f(\widehat{i}_{ma,b}(t), i_{mb}(t), i_{mc}(t)) \tag{23}$$

TABLE 3. PMSM parameters.

Parameters	Value (Unit)
DC link voltage V_{DC}	12 (V)
Stator resistance R_m	0.0186 (Ω)
d-axis stator inductance L_d	161.6 (uH)
q-axis stator inductance L_q	201.6 (uH)
Back EMF constant K_e	0.0417 (Vs/rad)
Pole pairs P	3

$$r_{ib,a\_c,b,c} = f(\widehat{i}_{ma,c}(t), i_{mb}(t), i_{mc}(t)) \tag{24}$$

The sensor fault isolation is performed based on the above six DC link battery current residuals. For example, if only r_{ib,a,b,c_a} out of these six residuals is less than δ_{ib}, it is the co-existence of phase B non-sensor imbalance fault and phase C sensor fault. This is because of that the phase C sensor measurement is replaced by a correct estimation with phase A sensor signal and the phase B non-sensor imbalance does not break the power conservation equation in the machine system. In this fault scenario, all other DC link battery current residuals other than r_{ib,a,b,c_a} would exceed δ_{ib}. For other similar co-existence fault scenarios, the isolation process could be performed similarly according to these different DC link battery current residuals.

C. SELECTED THRESHOLDS

The thresholds δ_{ib} and δ_{im} are obtained by checking the DC link battery current residual and phase current residuals at no-fault condition under PMSM full speed and load operating range. Residuals are calculated with correct sensor measurement to determine their normal variation range, based on which FDI thresholds are selected to tolerate the influence of noise, measurement error and system parameter drift. In this work, the thresholds δ_{ib} and δ_{im} are selected as 5% and 7.5% of the measured DC link current and phase current amplitude respectively. With a wide range of speed and torque, the normal variation of DC link battery current residual and phase current residuals will present a broader range which results in a higher δ_{ib} and δ_{im} values in order to secure their robustness, as compared to lower thresholds in the case with a limited range of speed and torque variations.

III. SIMULATION RESULTS AND DISCUSSION

Simulation work is carried out with MATLAB in order to validate the proposed machine current sensor FDI method. The simulation settings are selected to match the practice as close as possible. The PMSM system parameters are given in Table 3 which are obtained from a real vehicle motor. Single machine current sensor fault, multiple machine current sensor faults and single non-sensor fault are investigated. The PMSM is operating under changing load and changing speed conditions in which the machine current amplitude is varying depending on load requirements.

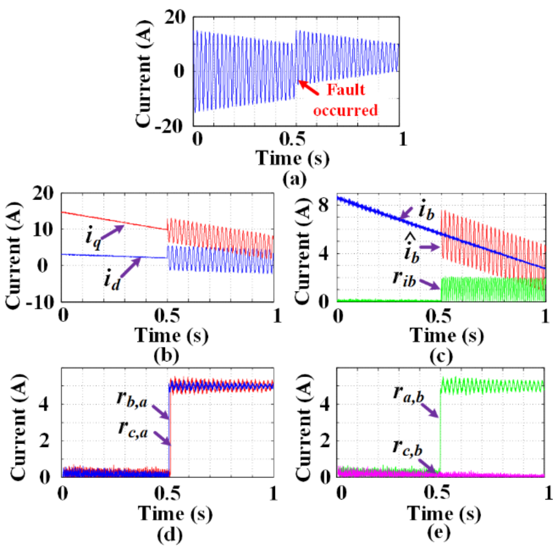

FIGURE 4. FDI for PMSM phase A current sensor fixed +5A offset fault from t =0.5s: (a) faulty PMSM phase A current sensor signal, (b) PMSM d-axis and q-axis currents, (c) measured and estimated DC link battery currents and residual r_{ib}, (d) current residuals $r_{b,a}$ and $r_{c,a}$, and (e) current residuals $r_{a,b}$ and $r_{c,b}$.

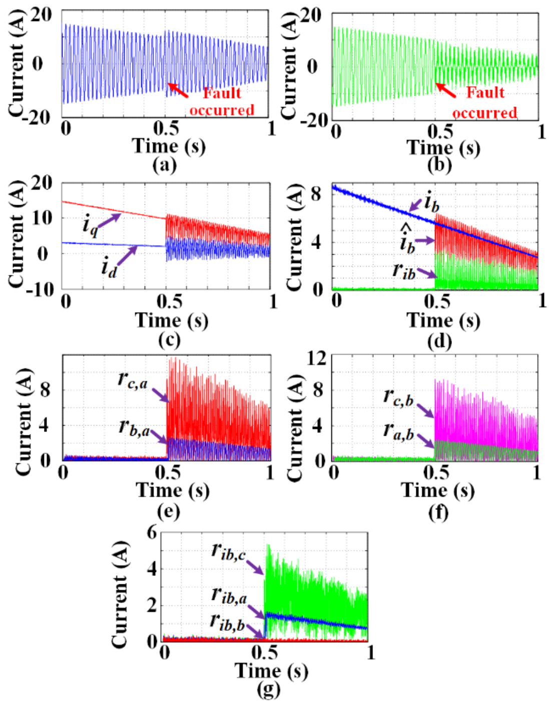

FIGURE 5. FDI for PMSM phase A current sensor 125% fixed scale and phase C current sensor random scale faults from t =0.5s: (a) faulty PMSM phase A current sensor signal, (b) faulty PMSM phase C current sensor signal, (c) PMSM d-axis and q-axis currents, (d) measured and estimated DC link battery currents and residual r_{ib}, (e) current residuals $r_{b,a}$ and $r_{c,a}$, and (f) current residuals $r_{a,b}$ and $r_{c,b}$, (g) $r_{ib,a}$, $r_{ib,b}$, and $r_{ib,c}$.

A. SINGLE SENSOR FDI

First, the single machine current sensor fault is studied. Fig. 4 shows the FDI for PMSM phase A current sensor fixed +5A offset fault. The fault occurs from t =0.5s as can be seen in Fig. 4(a) which leads to obvious dq-axis current oscillations in Fig. 4(b). These dq-axis current oscillations could be a challenge for the PMSM control system performance as well as the whole system stability if this fault is not well detected and isolated after its occurrence. The faulty current information from faulty sensor results in a wrong estimation of DC link battery current, and causes the estimated DC link current $\hat{i}_b$ deviating from the measurement value i_b, as shown in Fig. 4(c). With the proposed FDI method, the machine current sensor fault is timely detected based on the residual r_{ib} which increases significantly at t =0.5s, as illustrated in Fig. 4(c). This significant increase ofr_{ib} indicates a sensor fault occurrence. After the detection, the fault isolation is started and different phase signal residuals are examined. Since $r_{b,a}$ and $r_{c,a}$ all increase a lot at t =0.5s, as presented in Fig. 4(d), the fault scenario can be either phase A sensor fault or multiple-phase faults. However, further isolation reveals that there is a clear $r_{a,b}$ increase while $r_{c,b}$ stays close to zero, as shown in Fig. 4(e). Therefore, this is a single sensor fault. According to Table 2, this fault is well isolated as single machine current sensor fault in phase A.

B. MULTIPL SENSO FDI

The proposed method is able to handle multiple faults. The FDI results for PMSM phase A current sensor 125% fixed scale and phase C current sensor random scale faults are shown in Fig. 5. The faults happen from t =0.5s, as observed from phase A and C current waveforms in Fig. 5(a) and (b). The incorrect i_d and i_q, as presented in Fig. 5(c), will lead to chaotic pulse width modulation (PWM) signals in the inverter control. With the proposed FDI method, the faults are detected instantly after their occurrence according to r_{ib} in Fig. 5(d). In the following isolation stage, each of the residuals $r_{b,a}$, $r_{c,a}$, $r_{a,b}$ and $r_{c,b}$, as shown in Fig. 5(e) and (f), is found to present a significant increase, indicating this is a multiple faults scenario. Therefore, DC link battery current residual calculations based on single phase machine current sensor measurement are performed, and the calculated residuals $r_{ib,a}$, $r_{ib,b}$ and $r_{ib,c}$ are given in Fig. 5(g). It is clear in Fig. 5(g) that $r_{ib,b}$ remains close to zero after the sensor fault occurrence while $r_{ib,a}$ and $r_{ib,c}$ appear to have big value increases. The faults thereby are isolated in phase A and C current sensors.

Besides the two faults, the fault scenario with current sensor faults in all three phases are also investigated. FDI results for PMSM phase A, phase B and phase C current sensors random scale faults from t =0.5s are presented in Fig. 6. Similar fault detection process is implemented and the feature for fault occurrence are observed based on the DC link battery current residuals. Compared to the results presented in Fig. 5 with only two machine current sensor faults occurrence where one of the three recalculated DC link battery current residuals, i.e. $r_{ib,a}$, $r_{ib,b}$ and $r_{ib,c}$, stays close to zero after faults occurrence, these three residuals in Fig. 6 all increase significantly at t =0.5s. This is due

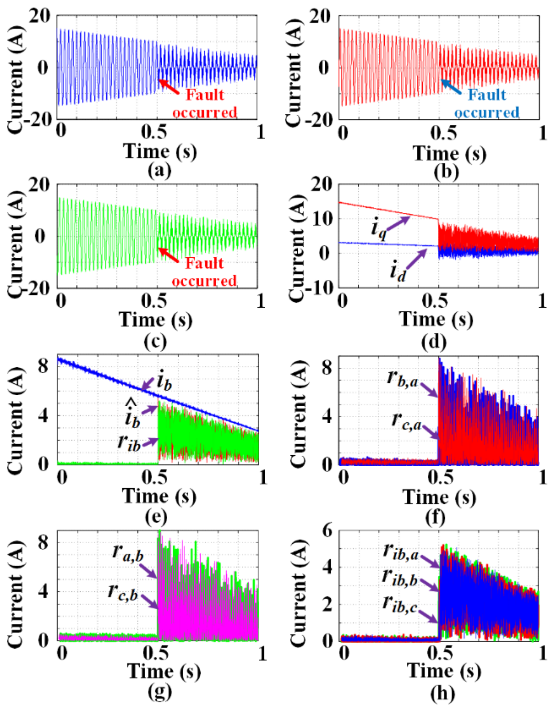

FIGURE 6. FDI for PMSM phase A, phase B and phase C current sensors random scale faults from t =0.5s: (a) faulty PMSM phase A current sensor signal, (b) faulty PMSM phase B current sensor signal, (c) faulty PMSM phase C current sensor signal, (d) PMSM d-axis and q-axis currents, (e) measured and estimated DC link battery currents and residual r_{ib}, (f) current residuals $r_{b,a}$ and $r_{c,a}$, and (g) current residuals $r_{a,b}$ and $r_{c,b}$, (h) $r_{ib,a}$, $r_{ib,b}$, and $r_{ib,c}$.

to the fact that none of the three machine current sensor measurements is correct and therefore recalculated DC link battery current residuals based on single phase machine current measurement will be all incorrect. Without considering sensor fault and non-sensor fault co-existence scenario, the results indicate that there are current sensor faults in all three phases.

C. NON-SENSOR FDI

The FDI results for PMSM phase C imbalance fault are given in Fig. 7. A phase C non-sensor imbalance fault occurs from t =0.5s, as shown in Fig. 7(a) t = 0.95 s, and the distorted dq-axis currents are plotted in Fig. 7(b). The DC link battery current residual in Fig. 7(c) is very close to zero, indicating there is no machine current sensor fault. However, the residuals $r_{c,a}$ and $r_{c,b}$ increase significantly while $r_{b,a}$ and $r_{a,b}$ keep close to zero, as can be seen from Fig. 7(d) and (e). Hence it can be inferred that a non-sensor imbalance fault has occurred in phase C.

The scenario with machine current sensor fault and non-sensor imbalance fault co-existence is covered as well, which is presented in Fig. 8. There is a phase B random scale non-sensor imbalance fault in addition to a phase C current sensor fixed -5A offset fault from t =0.5s, as shown in Fig. 8(a) and (b), respectively. The faults cause deeply

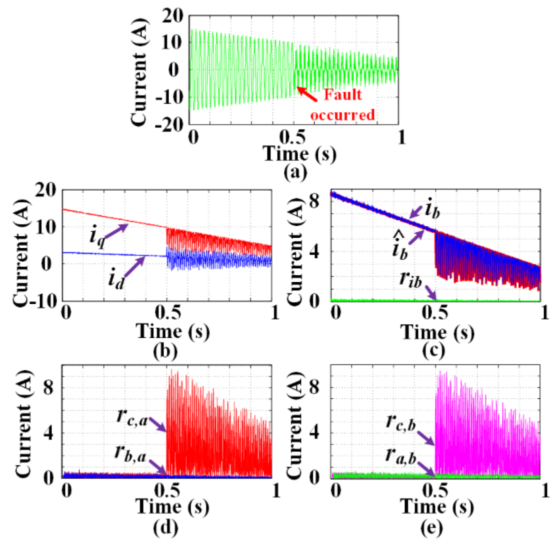

FIGURE 7. FDI for PMSM phase C random scale non-sensor (imbalance) fault from t =0.5s: (a) PMSM phase C current waveform under imbalance fault, (b) PMSM d-axis and q-axis currents, (c) measured and estimated DC link battery currents and residual r_{ib}, (d) current residuals $r_{b,a}$ and $r_{c,a}$, and (e) current residuals $r_{a,b}$ and $r_{c,b}$.

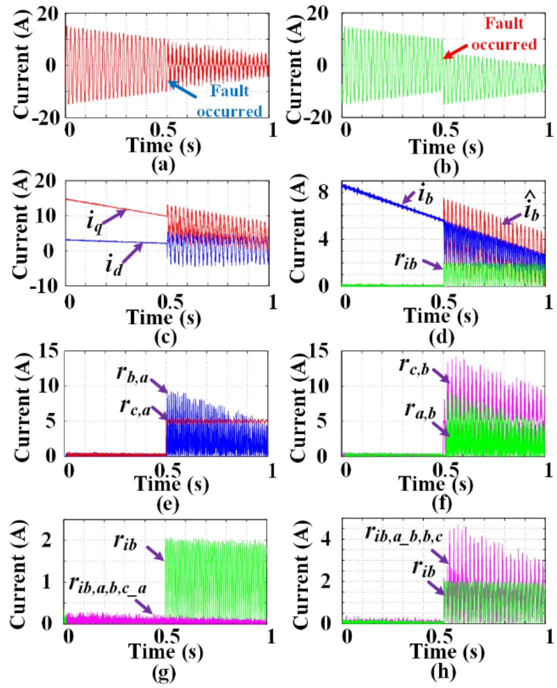

FIGURE 8. FDI for PMSM phase B random scale non-sensor imbalance fault and phase C current sensor fixed -5A offset fault from t =0.5s: (a) PMSM phase B current waveform under imbalance fault,(b) faulty PMSM phase C current sensor signal, (c) PMSM d-axis and q-axis currents, (d) measured and estimated DC link battery currents and residual r_{ib}, (e) current residuals $r_{b,a}$ and $r_{c,a}$, (f) current residuals $r_{a,b}$ and $r_{c,b}$, (g) r_{ib} and r_{ib,a,b,c_a}, and (h) r_{ib} and $r_{ib,a\_b,b,c}$.

oscillating dq-axis currents as well as the DC link battery current residual r_{ib}, as presented in Fig. 8(c) and (d). Based the proposed fault detection method, multiple faults are reported based on the four machine phase current residuals,

TABLE 4. Performance evaluation of proposed method for different sensor scale faults.

Threshold δ_{ib}	1%			2.5%			5%		
Fault scale	±20%	±10%	±5%	±10%	±7.5%	±5%	±20%	±15%	±10%
False detection rate F_D	84.32‱	81.50‱	89.69‱	0‱	0‱	0‱	0‱	0‱	0‱
Missed detection rate M_D	0%	0%	0%	0%	2.10%	100%	0%	1.79%	100%

as presented in Fig. 8(e) and (f), since all of them have significantly increased. In the following fault isolation process, the different DC link battery current residuals are calculated, such as $r_{ib,a\_b,b,c}$ and r_{ib,a,b,c_a} which are plotted in Fig. 8(g) and (h), respectively. It is clear from the figures that r_{ib,a,b,c_a} remains close to zero while $r_{ib,a\_b,b,c}$ does not. According to the fault isolation rules, the faults are accurately reported as phase B non-sensor imbalance fault and phase C machine current sensor fault.

D. DISCUSSIONS

Offset, fixed scale and random scale faults are chosen for the validation of the proposed machine current sensor FDI method in this work. Yet other types of fault, such as short time high, short time low, constant zero fault, could also be selected, and real-world faults, such as sensor measuring drift due to changing temperature or sensor signal missing, can be treated as one of the aforementioned fault scenarios or a mix of offset and scale errors. A severe fault in the machine system will return more noticeable features in the FDI results, which can be easily distinguished. When a fault is not severe, the detection result will be less noticeable, and could even dim out without difference compared to the no-fault condition. The minimum fault that can be detected with the proposed method is influenced by the system tolerance to false detection rate caused by error and noise. If a higher false detection rate could be tolerated, smaller fault will be detected. The performance evaluation of the proposed method in terms of false detection rate F_D and missed detection rate M_D for different scale faults is summarized in Table 4. The threshold value δ_{ib} has a significant influence on F_D and M_D. It can be seen that a small δ_{ib} =1% results in a high detection sensitivity, and even ±5% small scale faults are detected without any missed detection. However, this high sensitivity from a low threshold δ_{ib} also introduces a lot of false detections because the noise and errors cause certain level of DC link battery current residual r_{ib} value under no-fault condition. Increasing δ_{ib} makes the proposed more robust to noise and errors influence. For δ_{ib} =2.5% or 5%, no false detection exists with the proposed sensor FDI method in this work. On the other hand, a higher δ_{ib} will compromise the method sensitivity to small fault. For δ_{ib} =2.5%, there is 2.10% missed detections for ±7.5% scale faults, and 100% missed detections for ±5% or lower scale faults. When further increasing the threshold as δ_{ib} =5%, there is 1.79% missed detections for ±15% scale faults, and 100% missed detections for ±10% or lower scale faults. A high threshold value is selected when a system emphasizes more on a low false detection rate, compared to a high sensitivity to non-severe fault which sometimes is tolerable.

IV. CONCLUSION AND FUTURE WORK

A novel machine current sensor FDI method with a unique feature of being able to accurately detect and isolate multiple machine current sensor faults with the consideration of a non-sensor fault is proposed in this work. The fault detection is according to the residual between the estimated and measured DC link current, and the fault isolation is performed by residual examination based on phase signal estimation. The proposed method is not influenced by machine imbalance, has capability to handle both single and multiple machine current sensor faults, and has capability to distinguish between machine current sensor fault and non-sensor fault. The proposed method has been validated by various simulation studies with MATLAB. Future work could be conducted to study the machine current sensor fault-tolerant control after the sensor FDI, and the application of advanced algorithms, such as machine learning with feature extraction or pattern recognition, during the machine current sensor FDI.

REFERENCES

[1] B. Singh and S. Murshid, "A grid-interactive permanent-magnet synchronous motor-driven solar water-pumping system," *IEEE Trans. Ind. Appl.*, vol. 54, no. 5, pp. 5549–5561, Sep./Oct. 2018.
[2] X. Liang and C. Wang, "Factors affecting ground potential rise and fault currents along transmission lines with multigrounded shield wires," *IEEE Trans. Ind. Appl.*, vol. 53, no. 2, pp. 888–900, Mar./Apr. 2017.
[3] S. Hu, Y. Li, B. Xie, M. Chen, Z. Zhang, L. Luo, Y. Cao, A. Kubis, and C. Rehtanz, "A Y-D multifunction balance transformer-based power quality control system for single-phase power supply system," *IEEE Trans. Ind. Appl.*, vol. 52, no. 2, pp. 1270–1279, Mar./Apr. 2016.
[4] J. Ribrant and L. M. Bertling, "Survey of failures in wind power systems with focus on Swedish wind power plants during 1997–2005," *IEEE Trans. Energy Convers.*, vol. 22, no. 1, pp. 167–173, Mar. 2007.
[5] K. Rothenhagen and F. W. Fuchs, "Doubly fed induction generator model-based sensor fault detection and control loop reconfiguration," *IEEE Trans. Ind. Electron.*, vol. 56, no. 10, pp. 4229–4238, Oct. 2009.
[6] E. Kamal, A. Aitouche, R. Ghorbani, and M. Bayart, "Robust fuzzy fault-tolerant control of wind energy conversion systems subject to sensor faults," *IEEE Trans. Sustain. Energy*, vol. 3, no. 2, pp. 231–241, Apr. 2012.
[7] S. Rajendran, U. Govindarajan, S. Senthilvadivelu, and S. B. Uandai, "Intelligent sensor fault-tolerant control for variable speed wind electrical systems," *IET Power Electron.*, vol. 6, no. 7, pp. 1308–1319, Aug. 2013.
[8] M. E. H. Benbouzid, D. Diallo, and M. Zeraoulia, "Advanced fault-tolerant control of induction-motor drives for EV/HEV traction applications: From conventional to modern and intelligent control techniques," *IEEE Trans. Veh. Technol.*, vol. 56, no. 2, pp. 519–528, Mar. 2007.
[9] S. K. Kommuri, S. B. Lee, and K. C. Veluvolu, "Robust sensors-fault-tolerance with sliding mode estimation and control for PMSM drives," *IEEE/ASME Trans. Mechatronics*, vol. 23, no. 1, pp. 17–28, Feb. 2018.

[10] F. Mwasilu and J.-W. Jung, "Enhanced fault-tolerant control of interior PMSMs based on an adaptive EKF for EV traction applications," *IEEE Trans. Power Electron.*, vol. 31, no. 8, pp. 5746–5758, Aug. 2016.
[11] F. R. Salmasi, "A self-healing induction motor drive with model free sensor tampering and sensor fault detection, isolation, and compensation," *IEEE Trans. Ind. Electron.*, vol. 64, no. 8, pp. 6105–6115, Aug. 2017.
[12] B. Tabbache, N. Rizoug, M. El Hachemi Benbouzid, and A. Kheloui, "A control reconfiguration strategy for post-sensor FTC in induction motor-based EVs," *IEEE Trans. Veh. Technol.*, vol. 62, no. 3, pp. 965–971, Mar. 2013.
[13] Y. Yu, Y. Zhao, B. Wang, X. Huang, and D. Xu, "Current sensor fault diagnosis and tolerant control for VSI-based induction motor drives," *IEEE Trans. Power Electron.*, vol. 33, no. 5, pp. 4238–4248, May 2018.
[14] L. Guasch, F. Corcoles, and J. Pedra, "Effects of symmetrical and unsymmetrical voltage sags on induction machines," *IEEE Trans. Power Del.*, vol. 19, no. 2, pp. 774–782, Apr. 2004.
[15] Y.-S. Jeong, S.-K. Sul, S. E. Schulz, and N. R. Patel, "Fault detection and fault-tolerant control of interior permanent-magnet motor drive system for electric vehicle," *IEEE Trans. Ind. Appl.*, vol. 41, no. 1, pp. 46–51, Jan. 2005.
[16] H. Wang, S. Pekarek, and B. Fahimi, "Multilayer control of an induction motor drive: A strategic step for automotive applications," *IEEE Trans. Power Electron.*, vol. 21, no. 3, pp. 676–686, May 2006.
[17] C. Wu, C. Guo, Z. Xie, F. Ni, and H. Liu, "A signal-based fault detection and tolerance control method of current sensor for PMSM drive," *IEEE Trans. Ind. Electron.*, vol. 65, no. 12, pp. 9646–9657, Dec. 2018.
[18] I. Jlassi, J. O. Estima, S. K. El Khil, N. M. Bellaaj, and A. J. M. Cardoso, "A robust observer-based method for IGBTs and current sensors fault diagnosis in voltage-source inverters of PMSM drives," *IEEE Trans. Ind. Appl.*, vol. 53, no. 3, pp. 2894–2905, May/Jun. 2017.
[19] S. Saha, M. E. Haque, and M. A. Mahmud, "Diagnosis and mitigation of sensor malfunctioning in a permanent magnet synchronous generator based wind energy conversion system," *IEEE Trans. Energy Convers.*, vol. 33, no. 3, pp. 938–948, Sep. 2018.
[20] M. Manohar and S. Das, "Current sensor fault-tolerant control for direct torque control of induction motor drive using flux-linkage observer," *IEEE Trans. Ind. Informat.*, vol. 13, no. 6, pp. 2824–2833, Dec. 2017.
[21] B. Gou, Y. Xu, Y. Xia, G. Wilson, and S. Liu, "An intelligent time-adaptive data-driven method for sensor fault diagnosis in induction motor drive system," *IEEE Trans. Ind. Electron.*, vol. 66, no. 12, pp. 9817–9827, Dec. 2019.
[22] H. Li, Y. Qian, S. Asgarpoor, and H. Sharif, "PMSM current sensor FDI based on DC link current estimation," in *Proc. IEEE 88th Veh. Technol. Conf.*, Aug. 2018, pp. 1–5.
[23] H. Li, Y. Qian, S. Asgarpoor, and H. Sharif, "A sensor fault isolation scheme for co-existence of PMSM current sensor and non-sensor imbalance faults," in *Proc. IEEE Appl. Power Electron. Conf. Expo.*, Mar. 2019, pp. 2608–2613.
[24] *General Considerations: IGBT & IPM Modules*, Powerex, Chittoor, Andhra Pradesh, Jan. 2010.
[25] J. Li, G. Konstantinou, H. R. Wickramasinghe, J. Pou, X. Wu, and X. Jin, "Impact of circulating current control in capacitor voltage ripples of modular multilevel converters under grid imbalances," *IEEE Trans. Power Del.*, vol. 33, no. 3, pp. 1257–1267, Jun. 2018.
[26] D. Lopez-Perez and J. Antonino-Daviu, "Application of infrared thermography to failure detection in industrial induction motors: Case stories," *IEEE Trans. Ind. Appl.*, vol. 53, no. 3, pp. 1901–1908, May/Jun. 2017.

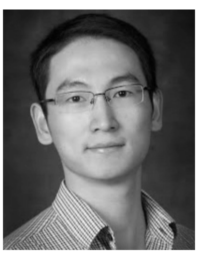

HAIBO LI (S'16) received the B.Eng. degree in electrical engineering from Anhui University, Hefei, China, in 2012. He is currently pursuing the part-time Ph.D. degree in electrical engineering with the University of Nebraska-Lincoln. He joined the University of Nebraska–Lincoln, in August 2013. He is currently an Applications Engineer with Power Integrations, San Jose, CA, USA. His research interests include electric motor drives, power electronics, and renewable energy.

YI QIAN (M'95–SM'07–F'19) is currently a Professor with the Department of Electrical and Computer Engineering, University of Nebraska-Lincoln (UNL), Lincoln, NE, USA. Prior to joining UNL, he worked in the telecommunications industry, academia, and the government. Some of his previous professional positions include serving as a Senior Member of the Scientific Staff, a Technical Advisor of Nortel Networks, a Senior Systems Engineer, a Technical Advisor with several start-up companies, an Assistant Professor with the University of Puerto Rico at Mayaguez, and a Senior Researcher with the National Institute of Standards and Technology. His research interests include information assurance and network security, network design, network modeling, simulation and performance analysis for next-generation wireless networks, wireless ad-hoc and sensor networks, vehicular networks, smart grid communication networks, broadband satellite networks, optical networks, high-speed networks, and the Internet. He was the Chair of the IEEE Communications Society Technical Committee for Communications and Information Security, from January 2014 to December 2015. He is the Technical Program Chair of the IEEE International Conference on Communications 2018. He is a Distinguished Lecturer of the IEEE Communications Society, and was a Distinguished Lecturer of the IEEE Vehicular Technology Society. He is serving on the editorial boards for several international journals and magazines, including serving as the Editor-in-Chief for the *IEEE Wireless Communications Magazine*.

SOHRAB ASGARPOOR (S'80–M'86–SM'91) received the B.S., M.S., and Ph.D. degrees in electrical engineering from Texas A&M University, College Station, TX, USA. From 1986 to 1989, he was with ABB Network Management Inc., as a Lead Engineer. Since September 1989, he has been with the University of Nebraska–Lincoln, Lincoln, NE, USA, where he is currently the Associate Dean of Undergraduate Programs with the College of Engineering, and a Professor with the Department of Electrical and Computer Engineering. His research interests include reliability evaluation, maintenance optimization, and advanced computer applications in security and optimization of power systems.

HAMID SHARIF (S'82–M'84–SM'06–F'17) is currently the Charles J. Vranek Distinguished Professor with the Department of Electrical and Computer Engineering, University of Nebraska–Lincoln. He is also the Director of the Advanced Telecommunications Engineering Laboratory (TEL), University of Nebraska. He has authored/coauthored more than 250 refereed research articles in international journals and conferences and has been a recipient of a number of research awards and best papers. His research interests include security in communication networks, wireless sensor networks, multimedia security, network modeling and simulations, and embedded systems. He has been serving on many editorial boards for the IEEE and other international journals. His research has been funded by major US government agencies and industries.